Burns & Trauma, 2025, **13**, tkae067
https://doi.org/10.1093/burnst/tkae067
Research Article

Zn ion-incorporated injected hydrogels with reactive oxygen species and glucose scavenging capacity for diabetic wound healing

Sicong Chen[1,2], Jiajun Qiu[2,*], Shuhan Chen[2], Xiaoshuang Nie[2], Linlin Zhao[3], Fang Wang[2], Hairong Liu[1,4,*], Xuanyong Liu[2,3,*]

[1]College of Material Science and Engineering, Hunan University, No. 2 Lushan South Road, Yuelu District, Changsha, Hunan 410082, P. R. China
[2]State Key Laboratory of High Performance Ceramics and Superfine Microstructure, Shanghai Institute of Ceramics, Chinese Academy of Sciences, No. 1295 Dingxi Road, Changning District, Shanghai 200050, P. R. China
[3]Shanghai Engineering Research Center of Nano-Biomaterials and Regenerative Medicine, College of Biological Science and Medical Engineering, Donghua University, No. 2999 Renmin North Road, Songjiang District, Shanghai 201620, P. R. China
[4]Hunan Regenerative Elements Biotechnology Co., Ltd, Unit G2-2, Lushan Science and Technology Innovation Park, No. 966 Lushan South Road, Yuelu District, Changsha, Hunan 410012, P. R. China

*Corresponding authors. X. Liu, Email: xyliu@mail.sic.ac.cn, H. Liu, Email: liuhairong@hnu.edu.cn, and J. Qiu, Email: qiujiajun@mail.sic.ac.cn

Abstract

Background: Patients with diabetic wounds often experience challenges in the repair process, owing to increased concentration of glucose and reactive oxygen species (ROS). In addition, high glucose levels usually result in bacterial infections, which in turn worsen wound healing. This study aims to develop a multifunctional hydrogel with integrated antibacterial activity, ROS scavenging, and glucose-responsive properties to accelerate healing of infected diabetic wounds.
Methods: A Zn ion-incorporated injected hydrogel was prepared using 4-carboxyphenylboronic acid-modified gelatine, tannic acid, and zinc ions. The spectra were detected using a Fourier transform infrared spectrometer and surface morphologies of hydrogels were obtained using a scanning electron microscopy. The release behavior of Zn ions was investigated using an inductively coupled plasma mass spectrometry instrument. To evaluate the antimicrobial properties of the GPT and GPT@Zn hydrogels, strains of *Escherichia coli* and *Staphylococcus aureus* were utilized. Cytocompatibility was evaluated using mouse fibroblasts (L929 cells) and human umbilical vein endothelial cells (HUVECs). Finally, diabetic wound models were constructed in rats to evaluate the effects of hydrogels on wound healing.
Results: The results show that the hydrogels are injectable and have self-healing properties. Moreover, borate ester bonds are formed in the hydrogels, which are responsive to H_2O_2 and glucose and can eliminate them. At the same time, zinc ions were released, giving the hydrogels good antibacterial efficacy, with antibacterial rates of 99.7% and 99.9% against *S. aureus* and *E. coli,* respectively. Furthermore, the hydrogels demonstrated good cell compatibility with L929 cells and HUVECs and increased the gene expression of VEGF, COL I, and COL III because of the addition of zinc ions. Based on the ROS, glucose scavenging capacity, and biological functions of zinc ions, the hydrogels advanced the recovery of *S. aureus*-contaminated whole skin wounds in diabetic rats.
Conclusions: This study provides a novel treatment strategy for diabetic wound healing by constructing Zn ion-incorporated injected hydrogels with reactive oxygen species and glucose-scavenging capacity.

Graphical Abstract

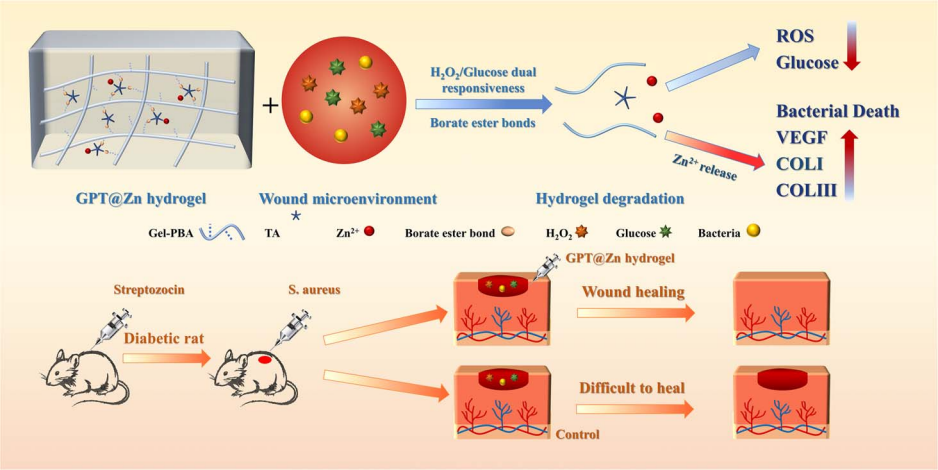

Received: April 15, 2024. **Revised:** October 7, 2024. **Accepted:** October 11, 2024

Keywords: Hydrogel; Borate ester bond; Reactive oxygen species; Antibacterial; Zn ions

Highlights

- A Zn ion-incorporated injected hydrogel composed of 4-carboxyphenylboronic acid-modified gelatine, tannic acid, and zinc ions (GPT@Zn) with reactive oxygen species and glucose scavenging capacity was prepared.
- The GPT@Zn hydrogels showed good antibacterial activity, with antibacterial rates of 99.7% and 99.9% against *S. aureus* and *E. coli*, respectively.
- The GPT@Zn hydrogels demonstrated good cell compatibility with L929 cells and HUVECs and increased the expression levels of key genes of VEGF, COL I, and COL III.
- The GPT@Zn hydrogels have the potential to advance satisfactory wound recovery for infectious diabetes full-thickness skin defects by promoting angiogenesis, enhancing collagen deposition, and inhibiting inflammation.

Introduction

As a natural barrier for the human body to resist external stimuli, the skin has important functions, such as safeguarding the body against injury and defending against microbial infiltration [1]. Due to its functions, the skin is easily damaged in the external environment, leading to the formation of wounds such as burns, ulcers, and infections. In addition, as skin wounds occur, a series of biological reactions are activated to restore the skin integrity and its functions [2, 3]. However, for diabetic wounds, wound repair is complex and difficult. Diabetes is a chronic disease, and patients' glycemic levels are generally high. High glucose levels in patients with diabetic wounds cause the expression of highly reactive oxygen species, which causes wounds to remain in a long-term inflammatory state. Moreover, high glucose levels also render wounds vulnerable to infection [4–7]. These situations cause disorders in the wound microenvironment and further lead to the inhibition of dermal and epidermal cell proliferation, angiogenesis obstacles, and skin regeneration difficulties in diabetic wounds [8–10]. Currently, diabetic wound healing in clinical practice still faces challenges.

Hydrogels are macromolecular polymers with 3D network cross-linking structures that have become very popular as wound dressings in recent years [11–13]. They are naturally soft and can absorb water, allowing them to swell and maintain a relatively fixed shape. They can soften wounds, cool them, and alleviate pain [14]. During the onset phase of diabetic wound recovery, the imbalance caused by bacterial infection and inflammatory reactions plays a pivotal role in the progression of chronic wounds. Therefore, functional hydrogel dressings can be applied at this stage to regulate the microenvironment for wound healing [7, 15, 16]. Therefore, researchers have devoted considerable effort to the development of functional hydrogels. Xu et al. prepared an Ag-containing antibacterial hydrogel for infected wound repair [17]. But the promotion of wound repair by simple antibacterial effects is limited. Recently, hydrogels with immunoregulatory functions have also been used to treat diabetic wounds. For example, a hydrogel with *Bletilla striata* polysaccharide could modulate the M1/M2 phenotype of macrophages and accelerate wound healing [18]. Moreover, hydrogels with microenvironments that diabetic wounds respond to have attracted widespread interest. Polyvinyl alcohol cross-linked with phenyl borate ester bonds was utilized to construct a reactive oxygen species-scavenging hydrogel. [19]. A smart system with glucose-mediated release of therapeutic agents was developed via Schiff base and phenyl boronate ester [20]. These reports suggest that phenyl borate ester bonds respond to the diabetic wound microenvironment and have potential applications in diabetic wound healing. Although functional hydrogels with antibacterial activity, immunoregulatory effects, and/or microenvironment responsiveness have been fabricated for wound healing, the construction of multifunctional hydrogels with reactive oxygen species and glucose scavenging capacity, as well as antibacterial activity for bacterial inhibition and diabetic wound healing, still faces a big challenge.

Gelatine is a natural collagen molecule with good biocompatibility [21, 22]. As a polyphenol, tannic acid (TA) has excellent antioxidant properties and can form borate ester bonds with phenylboronic acid bonds [23–25]. Borate ester bonds can react with H_2O_2 and glucose, presenting reactive oxygen species and glucose scavenging capacity [26–28]. Zinc ions have good antibacterial properties and other biological functions at appropriate concentrations, including promoting cell migration and collagen deposition [29, 30]. Based on these findings, we propose that a diabetic wound microenvironment -responsive hydrogel containing borate ester bonds and zinc ions with reactive oxygen species and glucose scavenging ability, and antibacterial activity, may have promising applications in bacteria-infected diabetic wound healing.

Therefore, in this work, reactive oxygen species and glucose-responsive hydrogels incorporating zinc ions were prepared. First, 4-carboxyphenylboronic acid was grafted onto the amino group of the gelatine. $ZnCl_2$ then reacted with TA to form a complex. Finally, the modified gelatine and complex were blended to form a hydrogel. The findings revealed that the hydrogels displayed self-healing and injectable capabilities. As borate ester bonds are formed, the hydrogels can react with ROS and glucose, presenting ROS and glucose scavenging capacity. The incorporation of zinc ions confers the hydrogels with superior antibacterial activities. An animal model of full-thickness skin wound in diabetic rats contaminated with *S. aureus* confirmed that the hydrogels accelerated the wound repair. This work proposes a novel treatment strategy for diabetic wound treatment by constructing Zn ion-containing hydrogels with reactive oxygen species and glucose scavenging capacity.

Methods

Preparation of Gel-PBA, TA-Zn, and GPT@Zn hydrogels

Gelatine modified with phenylboronic acid (Gel-PBA) was prepared via an amination reaction between -NH_2 on gelatine (Sigma–Aldrich, Germany) and -COOH on 4-carboxyphenylboronic acid (Adamas, Switzerland) [31, 32]. In detail, 4 g of gelatine was dissolved in 200 ml of deionized water. Next, 6 g of hydrochloride salt of N-(3-dimethylaminopropyl)-N'ethylcarbodiimide (EDC) (Sigma–Aldrich), 4 g of N-hydroxysuccinimide (NHS) (Sigma–Aldrich), and 1.5 g of 4-carboxyphenylboronic-acid were mixed in 80 ml of dimethyl sulfoxide for 2 h to activate the carboxyl groups [33], after which the as-prepared solution

was introduced into the gelatine solution and agitated at 37°C for a duration of 36 h. At Last, the compound was placed into a dialysis bag whose cut-off molecular weight is 6–8-kDa and subjected to dialysis in deionized water for 3 days with replacement every 12 h. Finally, Gel-PBA was obtained.

The TA and Zn ion mixture was then prepared as follows. Under vigorous stirring, 5 ml of $ZnCl_2$ (18 mg/ml) (Sinopharm Chemical Reagent Co., Ltd, China) was added into 5 ml of TA (30 mg/ml; Sigma–Aldrich, Germany) solution. After 2 h, a TA-Zn (TZ) solution was obtained. To obtain different mass ratios, different concentrations of $ZnCl_2$ (6 and 12 mg/ml) were used to prepare TZ solutions.

Finally, the hydrogel named Gel–PBA–TA (GPT) was fabricated by blending a 15% (W/V) Gel–PBA solution with a 1.5% (W/V) TA solution, which the volume ratio is 2:1. Gelation was achieved through the formation of a borate ester dynamic bond linking the PBA group in Gel–PBA with the gallate/catechol groups in TA [25]. Similarly, the TZ-containing hydrogel was named GPT@Zn, and different concentrations of zinc ions (0.1%, 0.2%, and 0.3% W/V) were introduced. The corresponding samples were denoted as GPT@Zn1, GPT@Zn2, and GPT@Zn3, respectively.

Characterization of the hydrogels

The structure confirmation of Gel-PBA was accomplished by ^{1}H NMR (minispec mq60, BRUKER OPTIK GMBH, Germany). The FTIR spectra of Gel-PBA, TA, and GPT were obtained via FTIR spectroscopy (Tensor 27, Bruker, Germany). The surface morphologies of GPT, GPT@Zn1, GPT@Zn2, and GPT@Zn3 were investigated by scanning electron microscopy (SEM, SU9000, Hitachi Limited, Japan).

H_2O_2 and glucose-responsive degradation behavior study

H_2O_2 and glucose-responsive degradation assessment was carried out in PBS, 0.6 mM H_2O_2, 4 g/L glucose, and 0.6 mM H_2O_2 + 4 g/L glucose solutions. Specifically, the GPT hydrogels (100 μl) were introduced into 1 ml of the aforementioned solutions, and the hydrogels were removed from the solution at 0, 1, 2, 3, 4, 6, 8, 12, 24, and 48 h. At last, mass residue rates of the hydrogels were then determined by weighing them after freeze-drying.

Zn ion release behavior assessment

The Zn ion release behaviors of the GPT@Zn1, GPT@Zn2, and GPT@Zn3 hydrogels were investigated in PBS solutions with or without 4 g/L glucose or 0.6 mM H_2O_2. Specifically, GPT@Zn1, GPT@Zn2, and GPT@Zn3 hydrogels (100 μl) were introduced into 1 ml of PBS solution with or without 4 g/L glucose or 0.6 mM H_2O_2, the supernatant was collected at 4, 12, 24, and 48 h, and 1 ml of fresh solution was then supplemented. Finally, the concentrations of Zn ions in the obtained solution were assessed via an inductively coupled plasma mass spectrometer (ICP-MS, NexION 2000, PerkinElmer, USA).

Rheological properties of the hydrogels

First, 0.6 ml of hydrogel was placed into the geometry gap of a rheometer (MCR301, Anton Paar, Austria). To verify the rheological properties of GPT, the frequency sweep was subsequently measured (5% strain), and the critical strain region of the GPT was quantitatively assessed across a range of amplitudes spanning at 1 Hz. The hydrogel's self-healing capabilities were evaluated through alternate step strain scanning examination at 1 Hz. The amplitude oscillation strain switching from a small strain (γ = 5%) to a subsequent large strain (γ = 300%) at a strain interval of 30 s was evaluated for three cycles.

Self-healing and injectability property assessment

First, 1 ml of hydrogel was divided into two parts and dyed blue or orange. Subsequently, the specimens were then positioned in a culture dish and maintained at ambient temperature for 5 min, after which their self-healing capacity was evaluated. Following the 5-min interval, the recovered hydrogel was carefully raised for observation. To assess the injectability, the dynamic hydrogel was placed into a 1-ml syringe, and the hydrogel in the syringe was squeezed into a culture dish to assess the extrusion capability of the GPT.

Antibacterial activity evaluation

The antibacterial activity evaluation was performed by coculture of hydrogel extracts with *E. coli* or *S. aureus*. First, 50 μl of hydrogel sample was immersed in 1 ml of sterile physiological saline, and the supernatant was collected to obtain the extract after 24 h. Subsequently, a mixture consisting of 500 μl of *E. coli* or *S. aureus* bacterial suspension (1.0×10^7 CFU/ml) and 500 μl of extraction solution was introduced into a 24-well plate, and 500 μl of sterile physiological saline was used as the blank control. Following an 8-h incubation period at 37°C, the sterile physiological saline was used to dilute the bacterial suspension and transferred to agar culture plates. Bacterial colonies from experimental groups (m_a) and the control group (m_0) after 12 h of cultivation was counted. The bacterial survival rate was obtained according to the following equation: survival rate (%) = $m_a/m_0 \times 100\%$.

To further assess the antibacterial efficacy of the GPT and GPT@Zn hydrogels, an inhibition ring assay was conducted. First, 100 μl of *S. aureus* or *E. coli* (1.0×10^7 CFU/ml) suspension was introduced onto agar culture plates, and then 50 μl of hydrogel was added and cultured at 37°C for 12 h. The widths of the suppression loops were measured separately.

Bacterial morphologies were observed according to the following method. First, glass slides were placed into a 24-well plate. Then, 500 μl of bacterial suspension (1.0×10^7 CFU/ml) and 500 μl of extraction solution were introduced, while 500 μl of sterile physiological saline served as a control. After an 8-h incubation period at 37°C, the bacteria upon the slides were dehydrated using different concentrations of alcohol (30, 50, 75, 90, 95, and 100 V/V%). At last, the SEM surface morphologies of bacteria were determined.

Hemolysis experiment

The hemocompatibility of the hydrogels was evaluated via the use of rat red blood cell (RBC) suspensions. Specifically, fresh rat blood was subjected to centrifugation at 3000 rpm for 5 min, then diluted to 2 v/v% with physiological saline. Five hundred microliters of 2% RBC solution and 500 μl of 0.05 g/ml hydrogel extracts were incubated at 37°C for 4 h. The group with deionized water added acted as the negative control, whereas group with physiological saline added served as the positive control. The mixed solution was centrifuged at 3000 rpm for 5 min, the absorbance at

a wavelength of 540 nm of the supernatant was quantified to determine the hemolysis rate of the hydrogels. The calculation of the hemolysis rate was performed via the following equation:

$$\text{Hemolysis rate } (\%) = \left(OD_{sample} - OD_{NaCl}\right) / \left(OD_{Water} - OD_{NaCl}\right) \times 100\%.$$

In vitro Cytocompatibility assessment

The Alamar blue (Gibco, USA) assay and LIVE/DEAD cell staining kit (Sigma–Aldrich) were employed for assessing the biocompatibility of the hydrogel extracts of GPT and GPT@Zn with L929 cells. Initially, the hydrogel (50 μl/ml) was immersed in α-MEM containing 10% fetal bovine serum (Gibco, USA) and cultured at 37°C for 24 h to obtain GPT and GPT@Zn extracts. For the assessment of cell viability, L929 cells at a density of 8.0×10^3 cells/well were introduced into a 96-well plate and cultured for 24 h, followed by replacement of the culture medium with hydrogel extract-containing culture medium and incubation for 24 and 48 h, followed by the addition of 100 μl of culture medium with 10% Alamar blue, allowing the cells to be cultured for a further 2 h. Finally, the absorbance of the supernatant was quantified via a microplate reader (Cytation 5; BIOTEK, USA). For LIVE/DEAD cell staining analysis, L929 cells were stained with calcein-AM and propidium iodide after being exposed to GPT and GPT@Zn hydrogel extracts for 24 h. Finally, fluorescence images were obtained. The biocompatibility of the GPT and GPT@Zn hydrogel extracts with HUVECs was evaluated via the same method.

DPPH free radical scavenging assessment

To investigate the ability of the GPT and GPT@Zn hydrogels scavenging DPPH radicals, DPPH solution with a concentration of 0.1 mM was prepared using ethanol. Subsequently, 50 μl of hydrogel was combined with 1 ml of ethanol (50 μl of PBS as a control group), and the mixture was kept in the dark at 37°C for 10 min, followed by the measurement of absorbance at a wavelength of 517 nm. The calculation of the DPPH radical scavenging rate of GPT and GPT@Zn was performed via the following equation:

$$\text{Scavenging effect } (\%) = \left(1 - OD_{sample}/OD_{control}\right) \times 100\%$$

ROS/hydrogen peroxide reactive fluorescence staining

To assess the capacity of GPT and GPT@Zn hydrogels eliminating hydrogen peroxide (H_2O_2), the H_2O_2 reactive fluorescent probe 2′,7′-dichlorodihydrofluorescein diacetate (DCFH-DA, 10 μM, Sigma–Aldrich) was employed to investigate the intracellular H_2O_2 levels after H_2O_2 treatment. In detail, L929 cells at a density of 3.0×10^4 cells/well were introduced into a 24-well plate and cultured for 24 h. Then, 1 ml of medium containing 0.6 mM H_2O_2 and 50 μl of hydrogel was introduced (50 μl of PBS serving as the control group) and cultured for another 6 h. Then, 500 μl of medium with 10% Alamar blue was introduced and cultured for another 2 h. The fluorescence intensity of the solutions was detected via a microplate reader. For LIVE/DEAD cell staining and DCFH-DA experiments, L929 cells treated with H_2O_2 and samples for 6 h were stained with calcein-AM, propidium iodide, and DCFH-DA. Fluorescence images were taken using a fluorescence microscopy.

In vitro RT–qPCR assessment

L929 cells (1.0×10^5 cells/well) were introduced into a 6-well plate and cultured for 24 h. Then, extraction solution-containing fresh culture medium was added and cultured for another 24 h. Subsequently, the cells were collected and Total RNA was extracted through cell lysis using TRIzol Reagent (Invitrogen, Thermo Fisher Scientific, Inc., USA). Complementary DNA (cDNA) was synthesized using a Transcriptor First-Strand cDNA Synthesis Kit (Roche, Switzerland). The housekeeping gene selected for normalization was glyceraldehyde-3-phosphate dehydrogenase (GAPDH), and the comparative expression analysis of the target genes was conducted using the $2^{-\Delta\Delta Ct}$ approach.

Animal experiments

The protocols for the use and care of the animals listed below were reviewed and approved by the Institutional Animal Care and Use Committee of Shanghai Rat & Mouse Biotech Co., Ltd. Sprague-Dawley (SD) rats were first induced to develop diabetes via a streptozotocin (STZ) solution. In detail, 6-week-old SD rats were adaptively fed for one week, subsequently receiving intraperitoneal injections of STZ at a dosage of 40 mg/kg of body weight, which the STZ was dissolved in a 1:1 mixture of 2.1 wt. % citric acid solution and 2.94 wt. % sodium citrate solution, with blood glucose levels measured every 3 days by collecting blood from the tail vein. When blood sugar stabilized above 16 mmol/L, the patient was considered hyperglycemic. When hyperglycemia stabilized for one week, the diabetic rat model was considered successful. The rats were then depilated with a razor and depilatory cream to expose the smooth skin. A circular blade was utilized to perform full-thickness excisions measuring 10 mm in diameter on their dorsal area. Two wounds were created in one rat, and each wound was introduced 20 μl (*S. aureus*, 1.0×10^7 CFU/ml) of bacterial mixture, after which 50 μl of hydrogel was administered to each wound. The wound healing conditions of the rat wounds on Days 1, 4, 7, and 14 were recorded.

One day after surgery, two rats from Control, TZ, GPT and GPT@Zn2 groups were sacrificed, and three wound tissue samples were gathered, diluted with sterile physiological saline, and placed on an agar culture plate. Bacteria colonies from experimental groups (m_a) and the control group (m_0) after 12 h of cultivation were counted. The bacterial survival rate was calculated according to the following equation: bacterial survival rate $(\%) = m_a/m_0 \times 100\%$. Another wound was stained with Giemsa to verify the infection status of the wound. On Days 7 and 14, the SD rats were euthanized to obtain the wound tissues, which were stored in 4% paraformaldehyde. Immunofluorescence assays were performed on the wound tissue for assessment of vascular endothelial growth factor (VEGF), platelet endothelial cell adhesion molecule (CD31), ROS, tumor necrosis factor alpha (TNF-α), and the anti-inflammatory factor interleukin-10 (IL-10). Histological evaluations of the wound tissues in SD rats were carried out using Masson's trichrome staining and hematoxylin-eosin (H&E) staining to examine the tissue changes.

Statistical analysis

The quantitative data are expressed as the means ± SDs. Statistical analysis was performed via one-way analysis of variance with GraphPad Prism 9.5.1 software. Statistical significance was set at $P < 0.05$. In all the cases, $^{*}P < 0.05$, $^{**}P < 0.01$, $^{***}P < 0.001$, and $^{****}P < 0.0001$.

Results

Fabrication and characterization of hydrogels

Gelatine is a natural collagen molecule, which contains multitudinous amino groups within its molecular chain. It can be grafted onto PBA molecules through amide reactions under the activation of EDC and NHS, resulting in Gel-PBA. The structures of Gel-PBA and Gel were characterized via ^{1}H NMR spectroscopy. As illustrated in Figure 1a, compared with that of Gel, a new peak appeared in the ^{1}H NMR spectrum of Gel-PBA at 7.3–7.8 ppm, which belongs to the benzene ring peak in PBA [34]. This indicates that PBA was successfully grafted onto gelatine. The chemical structures of the Gel-PBA, TA, and GPT hydrogels were characterized via FTIR spectroscopy, and the results are shown in Figure 1b. Compared with those of Gel-PBA, GPT displays absorption peaks at 1436 cm^{-1} and 1332 cm^{-1}, corresponding to the asymmetric stretching relaxation of B-O-C, indicating the existence of a borate ester bond in the GPT hydrogel [27].

The hydrogel was gelatinized by a borate ester bond, which can react with H_2O_2 and glucose. To confirm this, the responses of the hydrogels to H_2O_2 and glucose environments were studied. As shown in Figure 1c, at 24 h, the residual masses of GPT in the PBS, 0.6 mM H_2O_2 + PBS, 4 g/L glucose + PBS, and 0.6 mM H_2O_2 + 4 g/L glucose + PBS solutions were 55.6%, 34.6%, 12.4%, and 0%, respectively. Glucose competes with TA for the phenylboronic acid group on Gel-PBA, leading to the destruction of the original borate ester crosslinking sites of the hydrogels, which accelerates their degradation. In addition, the borate ester bond reacts with H_2O_2, and the C–P bond breaks, accelerating the degradation of the hydrogels. The degradation rate of the hydrogel in a H_2O_2-containing environment was greater than that in a glucose-containing environment. When H_2O_2 and glucose coexist, the above two reactions occur simultaneously, which further accelerates the degradation process of the hydrogels. It indicates that the GPT hydrogel has H_2O_2 and glucose dual responsiveness. Based on these findings, in environments containing both H_2O_2 and glucose, the hydrogels respond to the environment and release Zn ions, which may achieve good antibacterial effects.

To further explore the internal network structures of the hydrogels, the hydrogels were freeze-dried, and their cross-sections were observed via SEM. As shown in Figure 1d, GPT, GPT@Zn1, GPT@Zn2, and GPT@Zn3 had many porous structures. This is because the borate bond and the dihydroxy group cross-link to constitute a 3D network structure, which is the characteristic structure of biomedical hydrogels and is conducive to the penetration of nutrients and cells [35]. Compared with the microstructures of all the hydrogels, the addition of zinc had no effect on the general structure. The elemental mapping results revealed that zinc was evenly distributed in the hydrogels and that the concentration of zinc increased with increasing TZ in the hydrogel, indicating the successful loading of zinc. The ion release rates (Fig. 1e–g) of the GTP@Zn1, GPT@Zn2, and GPT@Zn3 groups indicated that the release rate of zinc ions increased in H_2O_2 and glucose conditions, which also confirmed the response characteristics of hydrogels to H_2O_2 and glucose.

Self-healing, injectability, and rheological properties of hydrogels

Figure 2a displays the gelation process of the GPT hydrogel. As shown in Figure 2b, the GPT hydrogel was divided into two pieces and dyed orange and blue. Then, the two sections were placed in intimate contact. Three minutes later, the two pieces of hydrogels became a single piece, indicating the good self-healing property of the GPT hydrogel. As depicted in Figure 2c, the GPT hydrogel can be injected through a syringe, and the latter shape is maintained, indicating that the hydrogel has good injectability.

The rheological test results of the hydrogels are shown in Figure 2d and e, which confirmed hydrogel formation [36]. As shown in Figure 2f, a cross-strain scanning test was performed with an interval of 30 s. Under 5% strain, G' is greater than G‘, which indicates that it is in a stable gelled state under low strain. When the strain increases to 300%, both G' and G' decrease simultaneously, and the decreasing magnitude of G' is much larger than that of G", indicating that its cross-linked structure is destroyed under high strain. When the strain increases to 5%, both G' and G' recover rapidly. After four cycles, G' can still recover to 75% of the initial state, indicating that the GPT hydrogel has superior self-healing performance [37].

In vitro antibacterial activities

Figure 3a demonstrates that bacteria colonies in the GPT group decreased to a certain extent, and with the addition of Zn, the number of colonies from GPT@Zn1, GPT@Zn2, and GPT@Zn3 decreased significantly, especially for GPT@Zn3. This indicated that the introduction of Zn ions into the hydrogels improved their antibacterial effects. GPT@Zn3 had the most significant inhibitory effect on *S. aureus* and *E. coli*, with bactericidal rates of 99.7% and 99.9%, respectively (Figure 3b and c). The results of the bacteriostatic ring analysis revealed that the antibacterial performance of the GPT@Zn is mainly ascribed to the release of zinc ions (Figure 3d–f). Because the fluidity of different hydrogels is different, antibacterial performance is expressed by the width of the antibacterial ring. For *S. aureus*, the width of the antibacterial ring increased with increasing Zn concentration. For the GPT@Zn3 group, a significant antibacterial ring against *E. coli* was observed, whereas the antibacterial rings from GPT@Zn1 and GPT@Zn2 were not obvious. This may be because the fluidity of the GPT@Zn1 and GPT@Zn2 hydrogels led to overlap of the hydrogels and bacteriostatic ring areas. These findings suggest that the GPT@Zn3 hydrogel with the highest Zn concentration exhibited the best antibacterial performance. The morphological changes in bacteria treated with different hydrogel extracts were subsequently observed by scanning electron microscopy (Figure 3g). *S. aureus* from the control group was smooth and had a spherical structure, whereas the bacterial membrane was broken to different degrees in the GPT@Zn1, GPT@Zn2, and GPT@Zn3 groups, especially for GPT@Zn3, where a large amount of bacterial cytoplasm flowed out, leading to bacterial

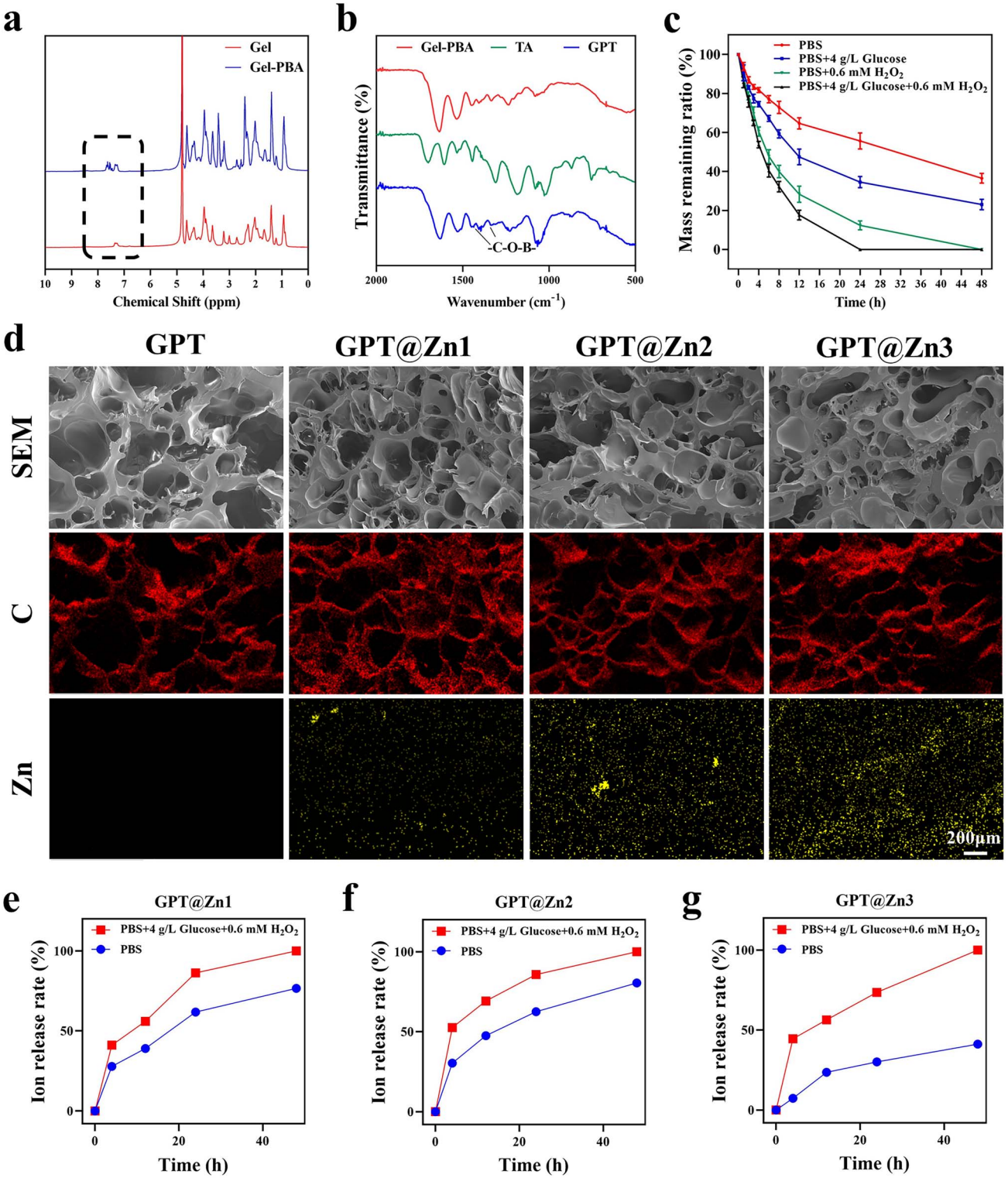

Figure 1. Hydrogel characterization. (**a**) ^{1}H NMR of Gel and Gel-PBA. (**b**) FTIR spectra of Gel-PBA, TA, and GPT. (**c**) the degradation curves of GPT hydrogels in PBS solution with or without glucose (4 g/L) and H_2O_2 (0.6 mM). (**d**) Surface morphologies of GPT, GPT@Zn1, GPT@Zn2, and GTPZ3 hydrogels and the distribution of C, Zn elements. Zn ion release curves of (**e**) GPT@Zn1, (**f**) GPT@Zn2, and (**g**) GTP@Zn3 hydrogels in PBS solution with or without glucose (4 g/L) and H_2O_2 (0.6 mM). *Gel* gelatin, *Gel-PBA* gelatine modified with phenylboronic acid, *TA* tannins acid, *GPT* hydrogel gelatinized by a borate ester bond, *GPT@Zn1*, *GPT@Zn2*, and *GPT@Zn3* hydrogels gelatinized by borate ester bond doped with Zn ions of different concentrations, *SEM* scanning electron microscope, *PBS* phosphate buffer solution

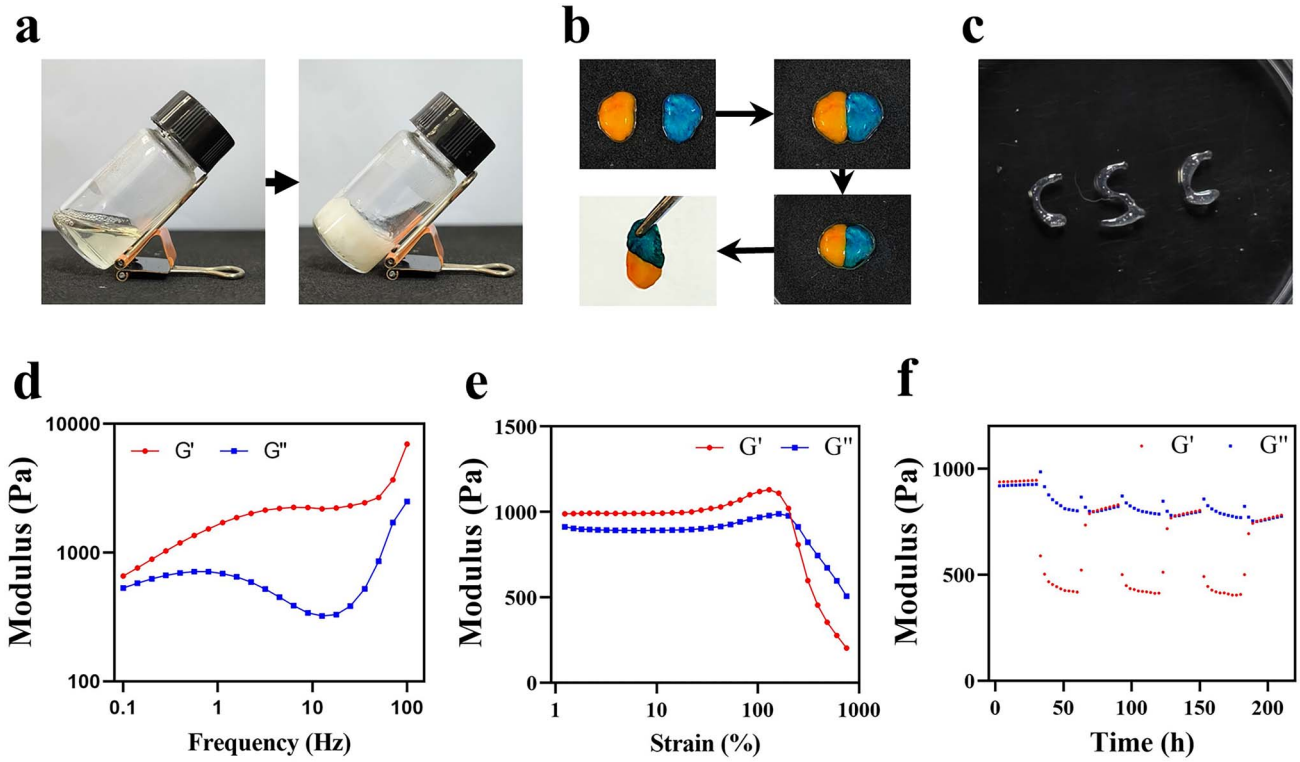

Figure 2. Physicohemical properties of the hydrogels. (**a**) Gelation process of GPT hydrogels. (**b**) Self-healing performance of GPT hydrogels. (**c**) Injectability performance of GPT hydrogels. (**d**) Variation in the loss modulus (G′) and storage modulus (G′) of the GPT hydrogel in frequency scanning mode. (**e**) Variation in the loss modulus (G′) and storage modulus (G′) of the GPT hydrogel in amplitude scanning mode. (**f**) G′ and G′ at alternate step strains of 5% and 300% for 60 s in each cycle (3 cycles). *G′* storage modulus, *G′* loss modulus

death. A similar trend was observed for *E. coli* in various samples.

Biocompatibility and hemolysis assessment

As depicted in Figure 4a, the viabilities of L929 cells cultured with GPT, GPT@Zn1, GPT@Zn2, and GPT@Zn3 for 24 and 48 h were > 95% compared with control group. Compared with GPT, the viability of L929 cells remained unchanged from GPT@Zn groups. For HUVECs, the cell activity of all the groups was above 90%, indicating good biocompatibility with HUVECs (Figure 4b). The results of live/dead cell staining assay are presented in Figure 4c. Green fluorescence with live cells was observed in all the samples, whereas no dead cells with red fluorescence was discernible. These findings suggest that GPT and GPT@Zn show biocompatibility with L929 cells and HUVECs.

The hemolytic toxicity of the four hydrogels was determined by measuring the hemolysis rate of red blood cells. According to the results in Figure 4d and e, the hemolysis rates of GPT, GPT@Zn1, GPT@Zn2, and GPT@Zn3 were lower than 1%, indicating the low hemolysis toxicity of the hydrogels [38].

In vitro anti-oxidative properties

The DPPH clearance rate reflects the overall antioxidant performance of a material [39]. The results of DPPH clearance *in vitro* revealed that the DPPH clearance rates of all the hydrogel groups exceeded 90%, suggesting that GPT and GPT@Zn possess excellent free radical scavenging abilities. (Figure 5a).

H_2O_2 is an important reactive oxygen species produced by chronic wounds [40]. Both borate esters and TAs can clear H_2O_2. To verify the ability of the hydrogels to eliminate H_2O_2, L929 cells were treated with H_2O_2-containing culture medium and various samples. DCFH-DA has cell permeability and no fluorescence but will be activated by intracellular H_2O_2 and converted into fluorescent products, enabling the detection of intracellular H_2O_2 levels. The results of the cell viability, ROS, and live/dead fluorescence staining revealed that in the H_2O_2-containing environment, high ROS levels in the H_2O_2 group can be observed with green fluorescence (Figure 5c), leading to low cell viability. However, when GPT or GPT@Zn2 was added, the green fluorescence of ROS was almost negligible, and the GPT and GPT@Zn2 groups exhibited better cell viability compared to the H_2O_2 group (Figure 5b). Notably, the addition of zinc ions to GPT@Zn2 had no effect on the antioxidant properties.

In vitro RT–qPCR assessment

VEGF is a commonly used biomarker for evaluating angiogenesis. COL I and COL III are vital members of the collagen family and represent the level of collagen deposition. The gene expression of VEGF, COL I, and COL III was investigated via RT–qPCR as presented in Figure 5d–f. GPT@Zn1, GPT@Zn2, and GPT@Zn3 exhibited enhanced gene expression of VEGF, especially in the GPT@Zn2 group, in comparison with control group. No remarkable disparity in VEGF expression was observed between the GPT and control groups. A similar rule was observed for the gene expression of COL I and COL III in various groups that GPT@Zn1, GPT@Zn2, and GPT@Zn3 showed enhanced gene expression, especially for

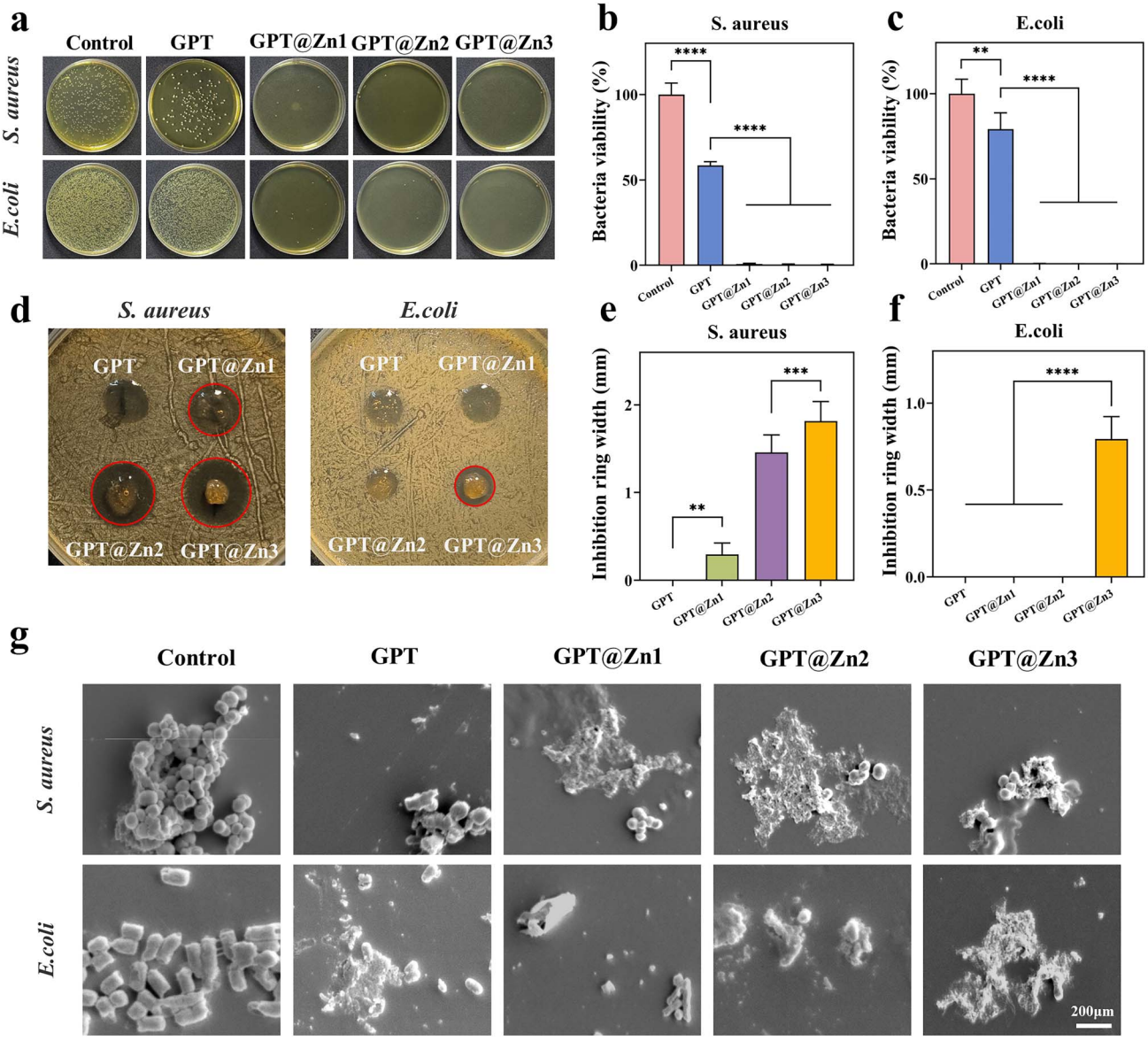

Figure 3. *In vitro* antibacterial properties of hydrogels. (**a**) Agar plates images of *E. Coli* and *S. Aureus* from control, GPT, GPT@Zn1, GPT@Zn2, and GPT@Zn3, and corresponding antibacterial rates of the hydrogels against (**b**) *E. Coli* and (**c**) *S. Aureus*. (**d**) Images of antibacterial ring against *E. Coli* and *S. Aureus* from GPT, GPT@Zn1, GPT@Zn2, and GPT@Zn3 and corresponding antibacterial ring width of the hydrogels against (**e**) *E. Coli* and (**f**) *S. Aureus*. (**g**) Bacterial morphologies of *E. Coli* and *S. Aureus* cultured on control, GPT, GPT@Zn1, GPT@Zn2, and GPT@Zn3. *GPT* hydrogel gelatinized by a borate ester bond, *GPT@Zn1, GPT@Zn2,* and *GPT@Zn3* hydrogels gelatinized by borate ester bond doped with Zn ions of different concentrations, *E. Coli Escherichia coli, S. Aureus Staphylococcus aureus*

the GPT@Zn2 group. This indicates that incorporating Zn ions plays a positive role in enhancing the expression of VEGF, COL I, and COL III. Based on the gene expression results, the GPT@Zn2 group was selected for subsequent animal experiments.

Wound healing and antibacterial activity *in vivo*

Photographs of infected diabetic wounds from various samples are illustrated in Figure 6a. The GPT@Zn2 group demonstrates a faster wound healing speed (Figure 6b). On the 4th day, the relative remaining wound areas in the control, TZ, GPT, and GPT@Zn2 groups were 52.6%, 45.3%, 43.3%, and 41.4%, respectively. A similar trend was observed on Days 7 and 14. These findings suggest that the GPT@Zn2 group exhibited the best wound healing state among these groups. The *in vivo* antibacterial experiments further confirmed that the zinc ion-containing groups, including TZ and GPT@Zn2, showed good antibacterial performance (Figure 6c and d). On the 1st day after surgery, Giemsa staining revealed that a biofilm had formed in the control group, bacteria were completely eliminated in the TZ and Zn groups, and bacteria were not completely eliminated in the GPT group Figure 6e, which is consistent with the *in vitro* and *in vivo* antibacterial results.

Collagen formation is an important indicator of wound healing. Collagen accumulation during wound healing was investigated via Masson staining. Optical images of collagen-stained wound tissues at 7 and 14 days after surgery are illustrated in Figure 7a. Collagen fibers are marked in blue,

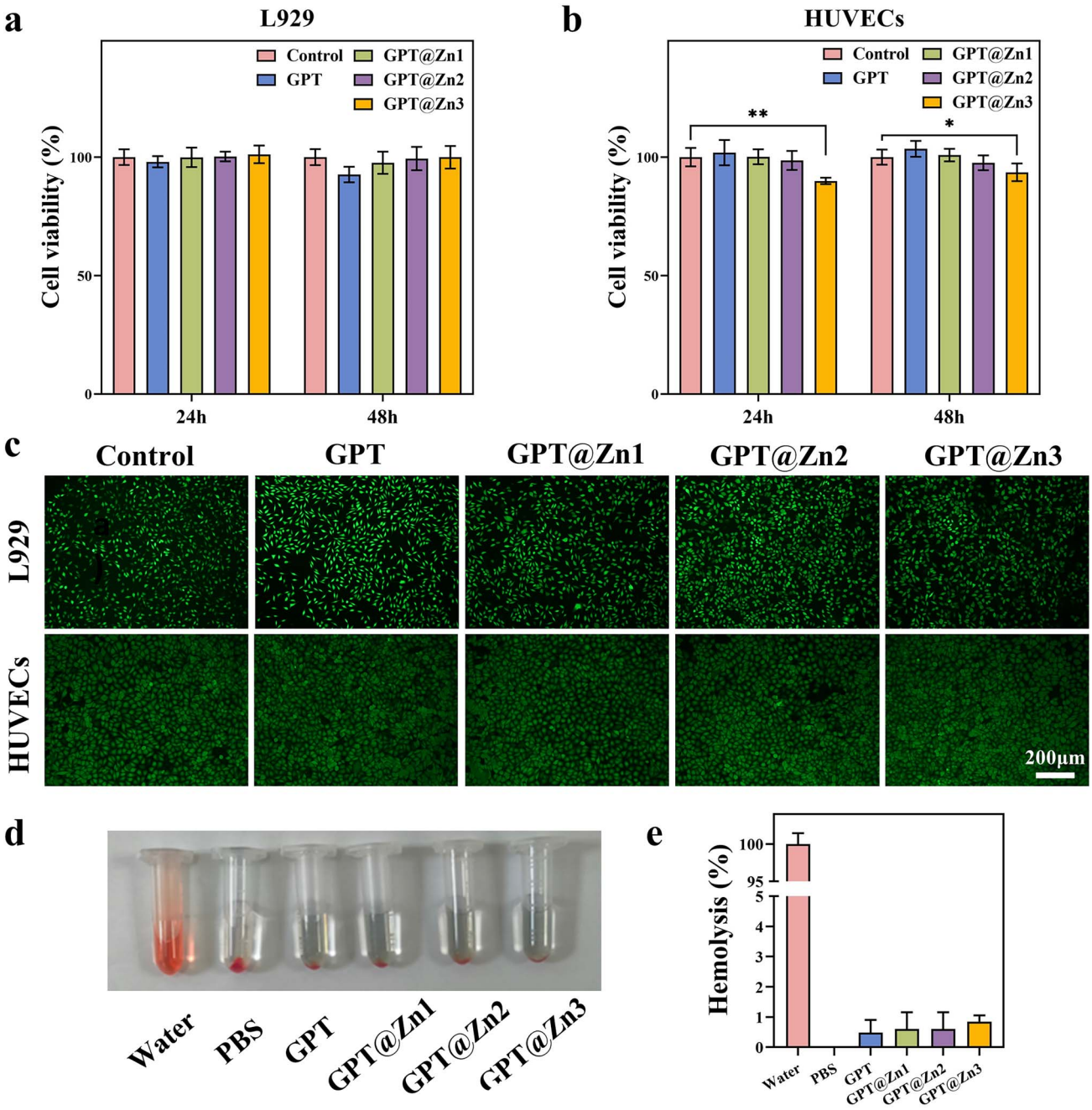

Figure 4. *In vitro* cytocompatibility and hemocompatibility of the hydrogels. (**a**) Cell viability of L929 cells incubated with GPT, GPT@Zn1, GPT@Zn2, and GPT@Zn3 extracts for 24 and 48 h. (**b**) Cell viability of HUVECs incubated with GPT, GPT@Zn1, GPT@Zn2, and GPT@Zn3 extracts for 24 and 48 h. (**c**) LIVE/DEAD staining of L929 cells and HUVEC incubated with GPT, GPT@Zn1, GPT@Zn2, and GPT@Zn3 extracts for 24 h. (**d**) Representative images of hemolysis results from various samples. (**e**) Hemolysis rates of various samples. *L929* mouse fibroblasts, *HUVECs* human umbilical vein endothelial cells, *GPT* hydrogel gelatinized by a borate ester bond, *GPT@Zn1, GPT@Zn2, GPT@Zn3* hydrogels gelatinized by borate ester bond doped with Zn ions of different concentrations, *PBS* phosphate buffer solution

and a certain amount of collagen deposition with blue colors was observed in the different groups, especially for GPT@Zn2. The quantitative results of collagen deposition on the 7th day after surgery shown in Figure 7b indicate that the percentages of collagen deposition in the control, TZ, GPT, and GPT@Zn2 groups were 40.1%, 50.1%, 45.6%, and 69.8%, respectively. The GPT@Zn2 group presented the highest level of collagen deposition. A similar trend was observed on the 14th day. These findings indicated that the GPT@Zn2 hydrogel promoted collagen deposition, thus promoting wound healing.

Immunohistochemical analysis of VEGF and CD31 was also performed, and the results are presented in Figure 7c–f. On the 7th day after surgery, the TZ, GPT, and GPT@Zn2 groups displayed higher expression of VEGF and CD31 in comparison with the control group. The GPT@Zn2 group presented the highest expression of VEGF and CD31. This may be attributed to the dual responsiveness of GPT@Zn2 to H_2O_2 and glucose, which can regulate the wound microenvironment and create conducive conditions for wound healing. Compared with GPT, higher expression of VEGF and CD31 could be found from GPT@Zn2, suggesting

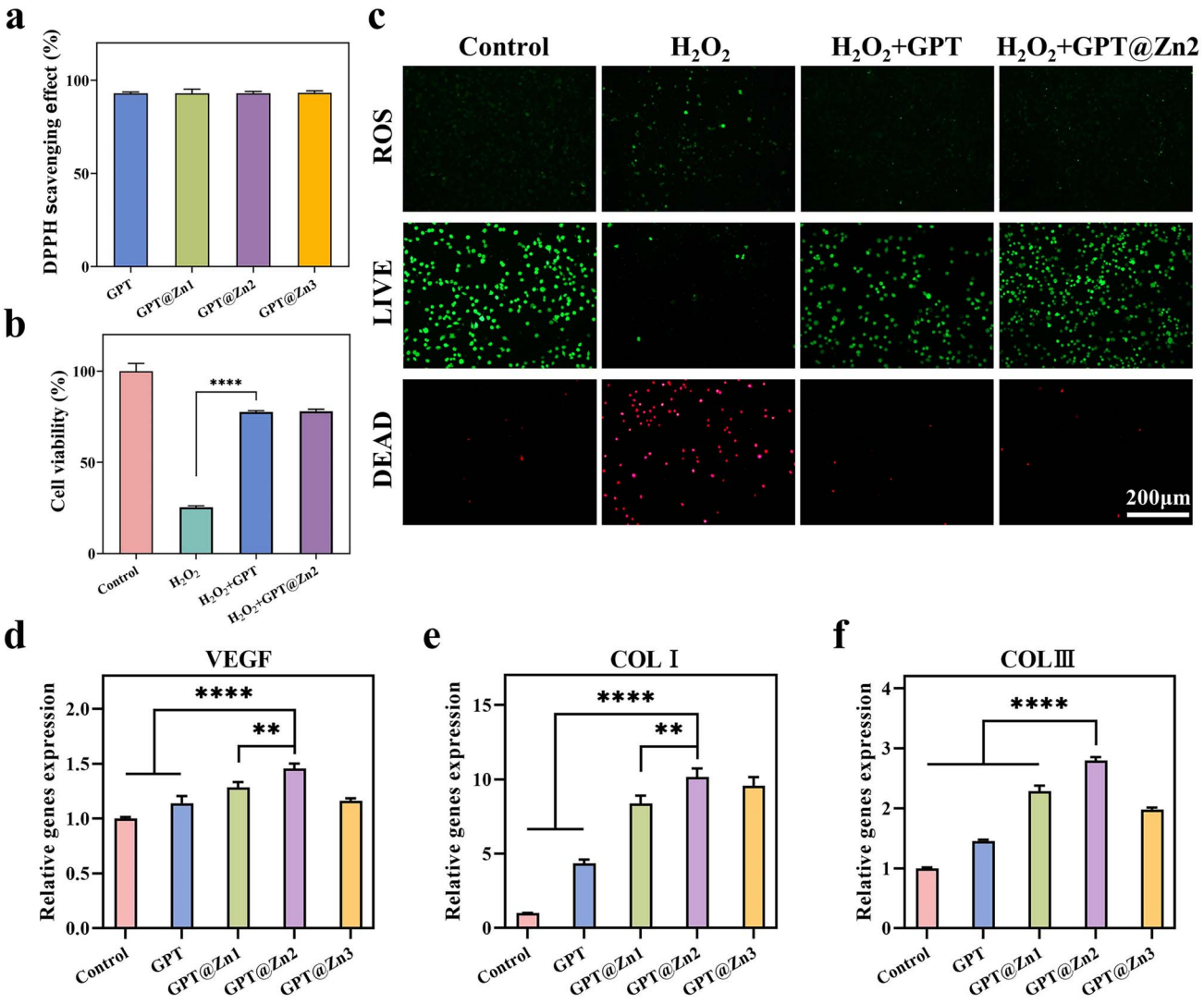

Figure 5. Antioxidative properties and real-time PCR analysis of hydrogels. (**a**) DPPH free-radical scavenging assay results for GPT, GPT@Zn1, GPT@Zn2, and GPT@Zn3. (**b**) Viability of L929 cells cultured with the control, H_2O_2 (0.6 mM), H_2O_2 + GPT and H_2O_2 + GPT@Zn2 groups. (**c**) Representative fluorescence images of ROS and LIVE/DEAD staining from the control, H_2O_2 (0.6 mM), H_2O_2 + GPT and H_2O_2 + GPT@Zn2 groups. Relative genes expression of (**d**) VEGF, (**e**) COL I, (**f**) COL III. *GPT* hydrogel gelatinized by a borate ester bond, *GPT@Zn1*, *GPT@Zn2*, and *GPT@Zn3* hydrogels gelatinized by borate ester bond doped with Zn ions of different concentrations, *VEGF* vascular endothelial growth factor, *COL I* collagen type I, *COL III* collagen type III, DPPH 2,2-Diphenyl-1-picrylhydrazyl, ROS reactive oxygen species

that the incorporation of Zn ions can also increase the expression of angiogenesis-related genes. On the 14th day after surgery, VEGF and CD31 expression decreased in response to GPT@Zn2, possibly because the wounds were repaired, and returned to normal levels [41].

Wound tissue healing efficacy was further assessed through H&E staining. As illustrated in Figure 8a, obvious inflammation was found in the control group but was markedly decreased in the TZ, GPT, and GPT@Zn2 groups on the 7th day, particularly in the GPT@Zn2 group, because of excellent antibacterial and antioxidant activity of GPT@Zn2.

The presence of acute inflammatory responses can result in heightened levels of reactive oxygen species within wounds, which can result in further injury to the tissue as well as hinder the healing process. Accordingly, the levels of ROS, the proinflammatory factor TNF-α, and the anti-inflammatory factor IL-10 were measured to further estimate the level of wound inflammation (Figure 8b–g). On the 7th day, the levels of ROS and TNF-α were reduced in the TZ, GPT, and GPT@Zn2 groups, whereas the expression of IL-10 was increased. These results indicate that GPT@Zn2 possesses remarkable potential to diminish wound inflammation and accelerate wound healing.

Discussion

Compared with normal wounds, diabetic wounds often do not heal as well. The wound repair process is significantly hindered by the complex and detrimental microenvironment of diabetic wounds, leading to the formation of chronic wounds [42]. In the present work, a novel wound dressing, GPT@Zn2, which can reduce high glucose and ROS levels in diabetic wounds, was developed to facilitate chronic diabetic wound healing.

Chronic diabetic wounds are accompanied with a high-glucose environment, which can easily cause microangiopathy and reduced neovascularization, serving as the initial factor for the formation of chronic diabetic wounds. Constant

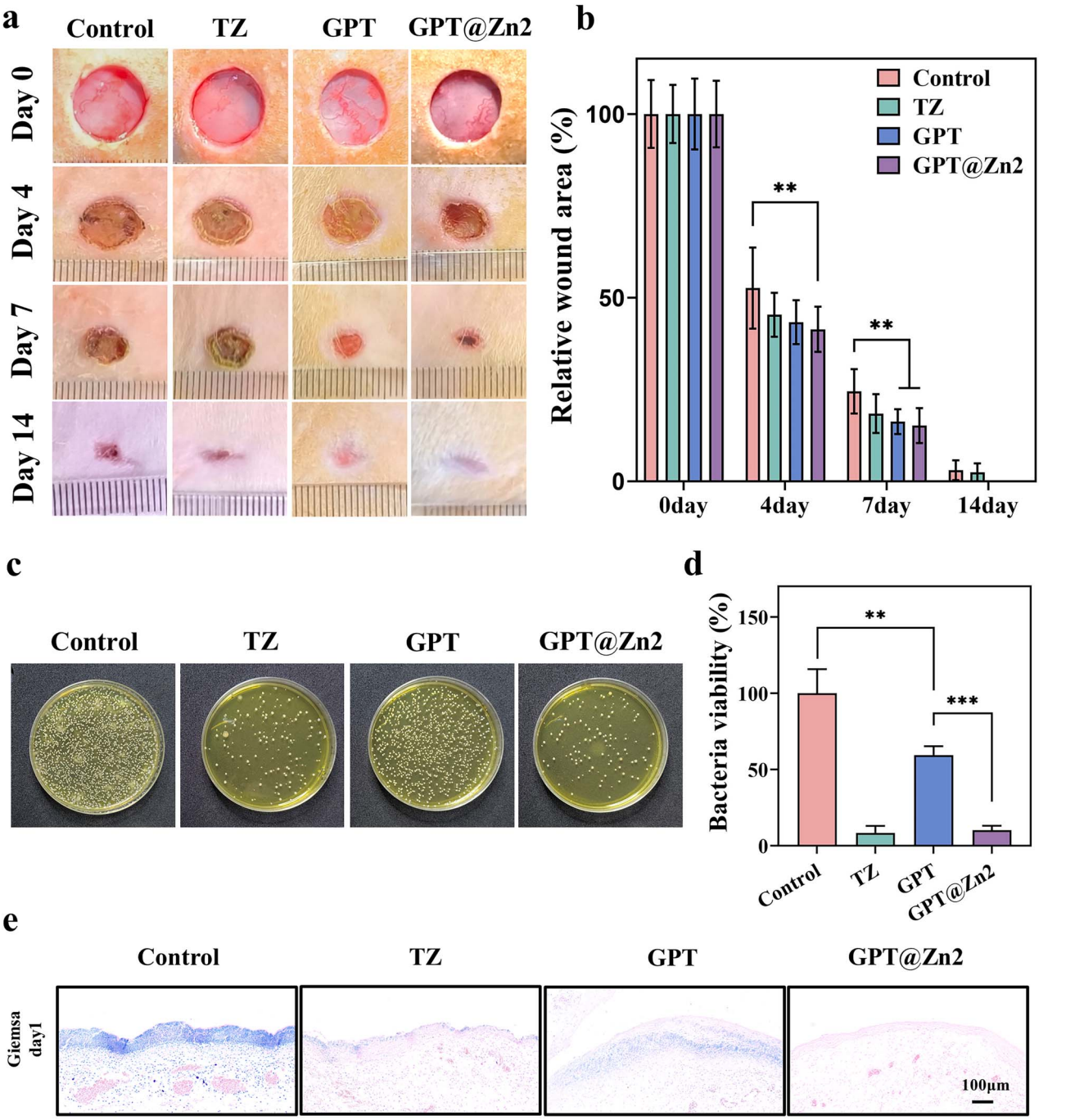

Figure 6. Wound closure evaluation and antibacterial properties of hydrogels *in vivo*. (**a**) Photographs of the wound healing site on Days 0, 4, 7, and 14, and (**b**) corresponding remaining wound area on Days 0, 4, 7, and 14. (**c**) Agar plate images of *S. Aureus* from control, TZ, GPT, and GPT@Zn2 groups, and (**d**) corresponding survival rates of *S. Aureus* from control, TZ, GPT, and GPT@Zn2 *groups in vivo*. (**e**) Giemsa staining of the control, TZ, GPT, and GPT@Zn2. *TZ* tannic acid and Zn ions solution, *GPT* hydrogel gelatinized by a borate ester bond, *GPT@Zn2* Zn ion-incorporated hydrogel gelatinized by a borate ester bond

exposure of wounds to a high-glucose environment can also lead to persistent inflammation. Additionally, the elevated glucose concentration within wounds can induce the production of excessive ROS, damaging bioactive factors including proteins and DNA, further stimulating wound inflammation, and eventually preventing wound repair [43]. Therefore, the removal of excess ROS is crucial. The GPT@Zn2 hydrogel can respond to and eliminate glucose and H_2O_2 within the microenvironment of diabetic wounds and has excellent DPPH scavenging ability. These findings indicated that the GPT@Zn2 hydrogel improved the wound microenvironment by scavenging ROS, thereby promoting wound healing.

As chronic diabetic wounds remain unhealed for a long time, they are constantly exposed, significantly increasing the risk of microbial infection. Wound infections caused by pathogens are difficult to eliminate through the immune response, which can further deteriorate the wound microenvironment, ultimately leading to wound ulceration

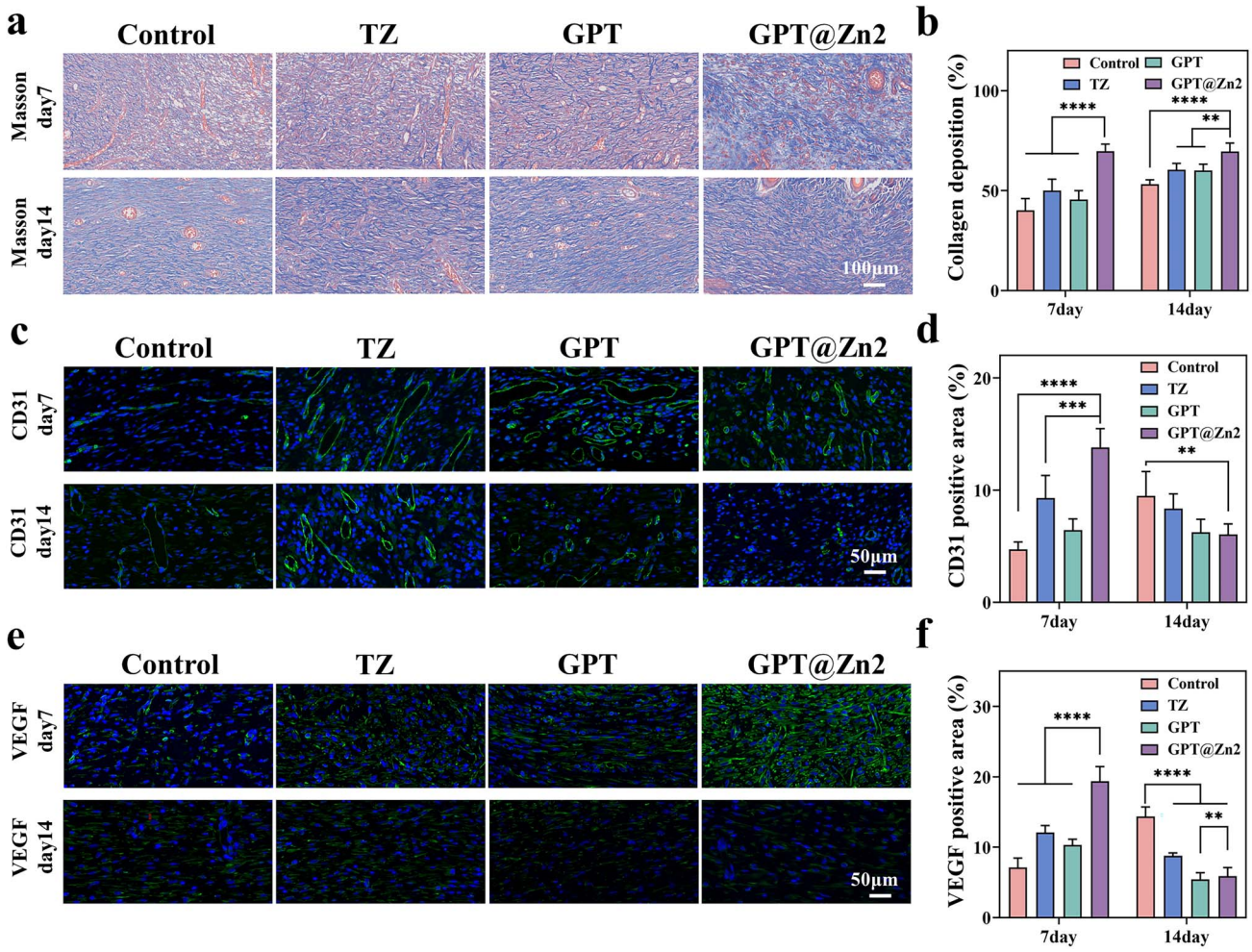

Figure 7. Histological evaluation of the wound tissue. (**a**) Masson staining images of wound tissues from the control, TZ, GPT, and GPT@Zn2 groups on Days 7 and 14, and (**b**) corresponding quantitative analysis of collagen deposition. (**c**) CD31 immunofluorescence staining images of wound tissues from control, TZ, GPT, and GPT@Zn2 groups on Days 7 and 14, and (**d**) corresponding quantitative analysis of CD31 positive areas. (**e**) VEGF immunofluorescence staining images of wound tissues from the control, TZ, GPT, and GPT@Zn2 groups on Days 7 and 14, and (**f**) corresponding quantitative analysis of VEGF-positive areas. *TZ* tannic acid and Zn ions solution, *GPT* hydrogel gelatinized by a borate ester bond, *GPT@Zn2* Zn ion-incorporated hydrogel gelatinized by a borate ester bond, *CD31* platelet endothelial cell adhesion molecule, *VEGF* vascular endothelial growth factor

[44]. Therefore, antibacterial properties are essential to ensure proper wound healing. The GPT@Zn2 hydrogel achieved good antibacterial effects by releasing zinc ions and inducing bacterial membrane disruption.

In addition, inflammation, angiogenesis, and collagen deposition are vital indicators for assessing the progress of wound healing. GPT@Zn2 hydrogel-treated wounds presented increased IL-10 and decreased TNF-α levels. These findings suggest that GPT@Zn2 advance the wound healing progress through inhibiting wound inflammation. The GPT@Zn2 hydrogel also promoted the secretion of VEGF, COL I, and COL III. After treatment with the GPT@Zn2 hydrogel, the VEGF and CD31 levels in the wound sites initially increased but then decreased, whereas the degree of collagen deposition increased. The results suggest that the GPT@Zn2 hydrogel enhances angiogenesis and collagen deposition during the wound repair process.

Above all, the GPT@Zn2 hydrogel can eliminate ROS and exhibit antibacterial properties, thereby improving the microenvironment of diabetic wounds, which is conducive to wound repair. In addition, GPT@Zn2 inhibits wound inflammation and promotes angiogenesis and collagen deposition, further facilitating wound healing. The GPT@Zn2 hydrogel is highly functional and has good application prospects for treatment of infectious chronic diabetic wounds.

Conclusions

To summarize, we constructed a Zn ion-incorporated hydrogel that displayed self-healing and injectable characteristics. Importantly, these hydrogels containing dynamic borate ester bonds could respond to diabetic wound microenvironments with high levels of reactive oxygen species and glucose concentrations, which exhibited reactive oxygen species and glucose scavenging capacity. In addition, zinc ions were added to the hydrogels as antibacterial agents, which endued the hydrogels good antibacterial properties. The results of the full-thickness skin wound model in diabetic rats contaminated with *S. aureus* confirmed that the hydrogels killed bacteria, promoted vascular regeneration and collagen deposition, which accelerated wound healing. Therefore, these Zn ion-incorporated injected hydrogels with reactive oxygen species and glucose scavenging capacity show promising applications for diabetic wound healing.

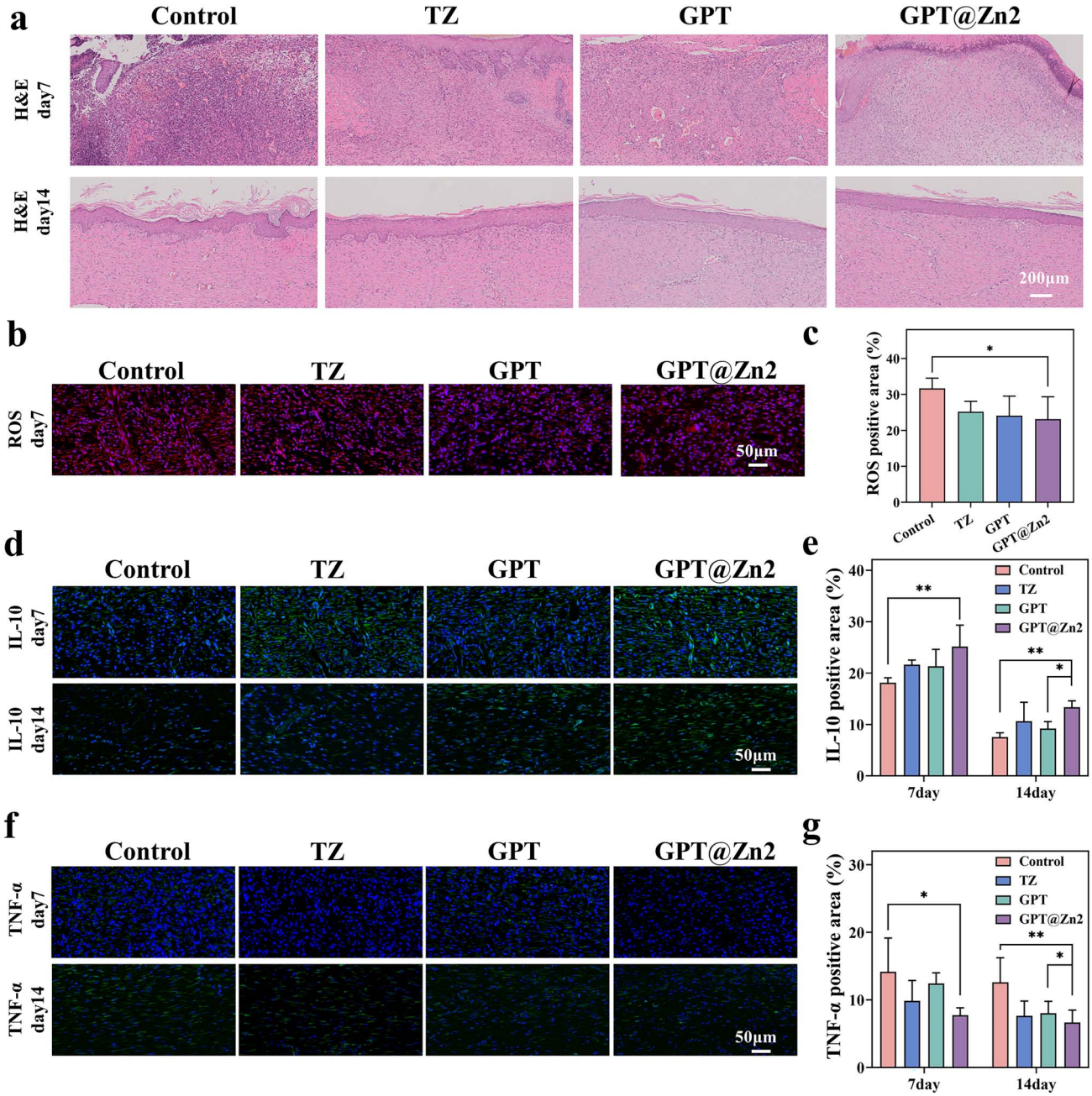

Figure 8. Histological evaluation of the wound tissue. (**a**) Hematoxylin–eosin staining images of wound tissues from control, TZ, GPT, and GPT@Zn2 groups on Days 7 and 14. (**b**) ROS immunofluorescence staining images of wound tissues from control, TZ, GPT, and GPT@Zn2 groups on Day 7, and (**c**) corresponding quantitative analysis of collagen deposition. (**d**) IL-10 immunofluorescence staining images of wound tissues from control, TZ, GPT, and GPT@Zn2 groups on Days 7 and 14 and (**e**) corresponding quantitative analysis of IL-10 positive areas. (**f**) TNF-α immunofluorescence staining images of wound tissues from control, TZ, GPT, and GPT@Zn2 groups on Days 7 and 14, and (**g**) corresponding quantitative analysis of TNF-α positive areas. *TZ* tannic acid and Zn ions solution, *GPT* hydrogel gelatinized by a borate ester bond, *GPT@Zn2* Zn ion-incorporated hydrogel gelatinized by a borate ester bond, *H&E* Hematoxylin-eosin, *ROS* reactive oxygen species, *IL-10* interleukin-10, *TNF-α* tumor necrosis factor alpha

Authors' contributions

Sicong Chen (Conceptualization [equal], Data Curation [equal], Investigation [equal], Validation [equal]), Jiajun Qiu (Formal Analysis [equal], Funding Acquisition [equal], Project Administration [equal], Resources [equal], Supervision [equal]), Shuhan Chen (Investigation [equal], Validation [equal]), Xiaoshuang Nie (Validation [equal]), Linlin Zhao(Validation [equal]), Fang Wang (Validation [equal]), Hairong Liu (Methodology [equal], Project Administration [equal]), Xuanyong Liu (Funding Acquisition [equal], Project Administration [equal], Resources [equal], Supervision [equal]).

Ethics approval and consent to participate

The animal study was approved by the Institutional Animal Care and Use Committee of Shanghai Rat & Mouse Biotech Co., Ltd (Number: RM202312(13)).

Funding

The work was financially supported by the National Key Research and Development Program of China (2022YFC2403000), Youth Innovation Promotion Association CAS (2023263), Young Elite

Scientists Sponsorship Program by CAST (2022-2024QNRC001), and Medical Key Subject of Xuhui District (SHXHZDXK202302).

Conflict of interest

The authors declare no conflict of interest.

Data availability

The data in the present study are available from the corresponding author upon reasonable request.

References

1. Schreml S, Szeimies RM, Karrer S, Heinlin J, Landthaler M, Babilas P. The impact of the pH value on skin integrity and cutaneous wound healing. *J Eur Acad Dermatol Venereol*. 2010;**24**:373–8. https://doi.org/10.1111/j.1468-3083.2009.03413.x.
2. Werdin F, Tenenhaus M, Rennekampff H-O. Chronic wound care. *Lancet*. 2008;**372**:1860–2. https://doi.org/10.1016/S0140-6736(08)61793-6.
3. Morton LM, Phillips TJ. Wound healing and treating wounds differential diagnosis and evaluation of chronic wounds. *J Am Acad Dermatol*. 2016;**74**:589–605. https://doi.org/10.1016/j.jaad.2015.08.068.
4. Ma Z, Song W, He Y, Li H. Multilayer injectable hydrogel system sequentially delivers bioactive substances for each wound healing stage. *ACS Appl Mater Interfaces*. 2020;**12**:29787–806. https://doi.org/10.1021/acsami.0c06360.
5. Wang H, Xu Z, Zhao M, Liu G, Wu J. Advances of hydrogel dressings in diabetic wounds. *Biomater Sci*. 2021;**9**:1530–46. https://doi.org/10.1039/D0BM01747G.
6. Kang SM, Cho H, Jeon D, Park SH, Shin DS, Heo CY. A matrix metalloproteinase sensing biosensor for the evaluation of chronic wounds. *Biochip J*. 2019;**13**:323–32. https://doi.org/10.1007/s13206-019-3403-4.
7. Kim YE, Kim J. ROS-scavenging therapeutic hydrogels for modulation of the inflammatory response. *ACS Appl Mater Interfaces*. 2022;**14**:23002–21. https://doi.org/10.1021/acsami.1c18261.
8. Eming SA, Martin P, Tomic-Canic M. Wound repair and regeneration: mechanisms, signaling, and translation. *Sci Transl Med*. 2014;**6**:3009337. https://doi.org/10.1126/scitranslmed.3009337.
9. Liu K, Kang Y, Dong X, Li Q, Wang Y, Wu X, *et al*. A simple yet effective hydrogel dressing for advanced microenvironmental management of diabetic wounds with intrinsic regulation. *Chem Eng J*. 2023;**470**:143987. https://doi.org/10.1016/j.cej.2023.143987.
10. Zhang Y, Zhu Y, Ma P, Wu H, Xiao D, Zhang Y, *et al*. Functional carbohydrate-based hydrogels for diabetic wound therapy. *Carbohydr Polym*. 2023;**312**:120823. https://doi.org/10.1016/j.carbpol.2023.120823.
11. Boateng J, Catanzano O. Advanced therapeutic dressings for effective wound HealingA review. *J Pharm Sci*. 2015;**104**:3653–80. https://doi.org/10.1002/jps.24610.
12. Brumberg V, Astrelina T, Malivanova T, Samoilov A. Modern wound dressings: hydrogel dressings. *Biomedicines*. 2021;**9**:9091235. https://doi.org/10.3390/biomedicines9091235.
13. Tavakoli S, Klar AS. Advanced hydrogels as wound dressings. *Biomol Ther*. 2020;**10**:10081169. https://doi.org/10.3390/biom10081169.
14. Yao H, Wu M, Lin L, Wu Z, Bae M, Park S, *et al*. Design strategies for adhesive hydrogels with natural antibacterial agents as wound dressings: status and trends. *Mater Today Bio*. 2022;**16**:100429. https://doi.org/10.1016/j.mtbio.2022.100429.
15. Wang Y, Wu Y, Long L, Yang L, Fu D, Hu C, *et al*. Inflammation-responsive drug-loaded hydrogels with sequential Hemostasis, antibacterial, and anti-inflammatory behavior for chronically infected diabetic wound treatment. *ACS Appl Mater Interfaces*. 2021;**13**:33584–99. https://doi.org/10.1021/acsami.1c09889.
16. Chen J, He J, Yang Y, Qiao L, Hu J, Zhang J, *et al*. Antibacterial adhesive self-healing hydrogels to promote diabetic wound healing. *Acta Biomater*. 2022;**146**:119–30. https://doi.org/10.1016/j.actbio.2022.04.041.
17. Xu G, Geng Y, Hu L, Wang J, Pan P, Chen J. One-pot preparation of polysaccharide-based antibacterial hydrogel for skin wound repair. *Macromol Mater Eng*. 2022;**307**:202100739. https://doi.org/10.1002/mame.202100739.
18. Liu J, Qu M, Wang C, Xue Y, Huang H, Chen Q, *et al*. A dual-cross-linked hydrogel patch for promoting diabetic wound healing. *Small*. 2022;**18**:202106172. https://doi.org/10.1002/smll.202106172.
19. Zhao H, Huang J, Li Y, Lv X, Zhou H, Wang H, *et al*. ROS-scavenging hydrogel to promote healing of bacteria infected diabetic wounds. *Biomaterials*. 2020;**258**:120286. https://doi.org/10.1016/j.biomaterials.2020.120286.
20. Zhao L, Niu L, Liang H, Tan H, Liu C, Zhu F. pH and glucose dual-responsive injectable hydrogels with insulin and fibroblasts as bioactive dressings for diabetic wound healing. *ACS Appl Mater Interfaces*. 2017;**9**:37563–74. https://doi.org/10.1021/acsami.7b09395.
21. Zhang Y, Chen H, Li J. Recent advances on gelatin methacrylate hydrogels with controlled microstructures for tissue engineering. *Int J Biol Macromol*. 2022;**221**:91–107. https://doi.org/10.1016/j.ijbiomac.2022.08.171.
22. Huang Y, Bai L, Yang Y, Yin Z, Guo B. Biodegradable gelatin/silver nanoparticle composite cryogel with excellent antibacterial and antibiofilm activity and hemostasis for *Pseudomonas aeruginosa*-infected burn wound healing. *J Colloid Interface Sci*. 2022;**608**:2278–89. https://doi.org/10.1016/j.jcis.2021.10.131.
23. Jafari H, Ghaffari-Bohlouli P, Niknezhad SV, Abedi A, Izadifar Z, Mohammadinejad R, *et al*. Tannic acid: a versatile polyphenol for design of biomedical hydrogels. *J Mater Chem B*. 2022;**10**:5873–912. https://doi.org/10.1039/D2TB01056A.
24. Jing W, Xiaolan C, Yu C, Feng Q, Haifeng Y. Pharmacological effects and mechanisms of tannic acid. *Biomed Pharmacother*. 2022;**154**:113561. https://doi.org/10.1016/j.biopha.2022.113561.
25. Wei Q, Zhao Y, Wei Y, Wang Y, Jin Z, Ma G, *et al*. Facile preparation of polyphenol-crosslinked chitosan-based hydrogels for cutaneous wound repair. *Int J Biol Macromol*. 2023;**228**:99–110. https://doi.org/10.1016/j.ijbiomac.2022.12.215.
26. Shi W, Kong Y, Su Y, Kuss MA, Jiang X, Li X, *et al*. Tannic acid-inspired, self-healing, and dual stimuli responsive dynamic hydrogel with potent antibacterial and anti-oxidative properties. *J Mater Chem B*. 2021;**9**:7182–95. https://doi.org/10.1039/D1TB00156F.
27. Deng CC, Brooks WLA, Abboud KA, Sumerlin BS. Boronic acid-based hydrogels undergo self-healing at neutral and acidic pH. *ACS Macro Lett*. 2015;**4**:220–4. https://doi.org/10.1021/acsmacrolett.5b00018.
28. Xie W, Zhang Y, Zhang J, Chen X, Pan J, Zhu X, *et al*. Dynamically crosslinked protien hydrogel composite as multifunctional wound dressing for cutaneous infection. *Colloid Interface Sci Commun*. 2022;**50**:100654. https://doi.org/10.1016/j.colcom.2022.100654.
29. Yuan Z, Wan Z, Tian Z, Han Y, Huang X, Feng Y, *et al*. In situ fused granular hydrogels with ultrastretchability, strong adhesion, and mutli-bioactivities for efficient chronic wound care. *Chem Eng J*. 2022;**450**:138076. https://doi.org/10.1016/j.cej.2022.138076.
30. Yang F, Xue Y, Wang F, Guo D, He Y, Zhao X, *et al*. Sustained release of magnesium and zinc ions synergistically accelerates wound healing. *Bioact Mater*. 2023;**26**:88–101. https://doi.org/10.1016/j.bioactmat.2023.02.019.
31. Tao B, Chen M, Lin C, Lu L, Yuan Z, Liu J, *et al*. Zn-incorporation with graphene oxide on Ti substrates surface to improve osteogenic activity and inhibit bacterial adhesion. *J Biomed Mater Res Part A*. 2019;**107**:2310–26. https://doi.org/10.1002/jbm.a.36740.

32. Nguyen HD, Sun X, Yokota H, Lin CC. Probing osteocyte functions in Gelatin hydrogels with Tunable viscoelasticity. *Biomacromolecules*. 2021;**22**:1115–26. https://doi.org/10.1021/acs.biomac.0c01476.
33. Liu L, Zhang X, Zhang Y, Pu Y, Yin L, Liu H, *et al*. Conjugation of antibody on carboxyl-SPIO nanoparticles based on EDC/sulfo-NHS. *Acta Univ Med Nanjing*. 2013;**33**:480–4.
34. Li C, Wu G, Ma R, Liu Y, Liu Y, Lv J, *et al*. Nitrilotriacetic acid (NTA) and Phenylboronic acid (PBA) functionalized Nanogels for efficient encapsulation and controlled release of insulin. *ACS Biomater Sci Eng*. 2018;**4**:2007–17. https://doi.org/10.1021/acsbiomaterials.7b00546.
35. Jayakumar A, Jose VK, Lee JM. Hydrogels for medical and environmental applications. *Small Methods*. 2020;**4**:201900735. https://doi.org/10.1002/smtd.201900735.
36. Roberts MC, Hanson MC, Massey AP, Karren EA, Kiser PF. Dynamically restructuring hydrogel networks formed with reversible covalent crosslinks. *Adv Mater*. 2007;**19**:2503–7. https://doi.org/10.1002/adma.200602649.
37. Chen MH, Wang LL, Chung JJ, Kim YH, Atluri P, Burdick JA. Methods to assess shear-thinning hydrogels for application As injectable biomaterials. *ACS Biomater Sci Eng*. 2017;**3**:3146–60. https://doi.org/10.1021/acsbiomaterials.7b00734.
38. Henkelman S, Rakhorst G, Blanton J, van Oeveren W. Standardization of incubation conditions for hemolysis testing of biomaterials. *Mater Sci Eng C*. 2009;**29**:1650–4. https://doi.org/10.1016/j.msec.2009.01.002.
39. Zhu Y, Matsumura Y, Velayutham M, Foley LM, Hitchens TK, Wagner WR. Reactive oxygen species scavenging with a biodegradable, thermally responsive hydrogel compatible with soft tissue injection. *Biomaterials*. 2018;**177**:98–112. https://doi.org/10.1016/j.biomaterials.2018.05.044.
40. Dhall S, Do DC, Garcia M, Kim J, Mirebrahim SH, Lyubovitsky J, *et al*. Generating and reversing chronic wounds in diabetic mice by manipulating wound redox parameters. *J Diabetes Res*. 2014;**2014**:1–18. https://doi.org/10.1155/2014/562625.
41. Korntner S, Lehner C, Gehwolf R, Wagner A, Grütz M, Kunkel N, *et al*. Limiting angiogenesis to modulate scar formation. *Adv Drug Deliv Rev*. 2019;**146**:170–89. https://doi.org/10.1016/j.addr.2018.02.010.
42. Zhang S, Ge G, Qin Y, Li W, Dong J, Mei J, *et al*. Recent advances in responsive hydrogels for diabetic wound healing. *Mater Today Bio*2023. 2022;**18**:100508. https://doi.org/10.1016/j.mtbio.2022.100508.
43. Chen Y, Wang X, Tao S, Wang Q, Ma PQ, Li ZB, *et al*. Research advances in smart responsive-hydrogel dressings with potential clinical diabetic wound healing properties. *Mil Med Res*. 2023;**10**:s40779-023-00473-9. https://doi.org/10.1186/s40779-023-00473-9.
44. Falanga V, Isseroff RR, Soulika AM, Romanelli M, Margolis D, Kapp S, *et al*. Chronic wounds. *Nat Rev Dis Primers*. 2022;**8**:s41572-022-00377-3. https://doi.org/10.1038/s41572-022-00377-3.

Burns & Trauma, 2025, 13, tkae067
https://doi.org/10.1093/burnst/tkae067
Research Article